Research article

Crosstalk of cuproptosis-related subtypes, establishment of a prognostic signature, and immune infiltration characteristics in gastric cancer

Yatao Wang [a,1], Fengqin Guo [b,1], Wei Song [a,1], Wenyi Guo [a], Junwei Shao [a], Yanliang Liu [a,*]

[a] Department of Gastrointestinal Surgery II, Renmin Hospital of Wuhan University, Wuhan, Hubei, 430060, China
[b] Department of Obstetrics & Gynecology, Renmin Hospital of Wuhan University, Wuhan, Hubei, 430060, China

ABSTRACT

Background: Cuproptosis is a novel form of cellular demise that occurs through a unique pathway involving lipoylated proteins in the tricarboxylic acid (TCA) cycle and is closely linked to mitochondrial metabolism. Nevertheless, the comprehensive elucidation of the impact of carcinogenesis-associated genes (CRGs) on prognosis, tumor microenvironment (TME), and therapeutic response in patients with gastric cancer (GC) remains unclear.
Methods: In total, 1374 GC samples were gathered from three Gene Expression Omnibus (GEO) datasets and The Cancer Genome Atlas database. The samples were then stratified into different subtypes through unsupervised clustering of the 13 CRG profiles. The CRG_score was developed to quantify CRG patterns of individual tumors. Subsequently, we investigated the associations among the various groups and clinicopathological features, immune infiltration features, TME mutation status, and response to immunotherapy.
Results: The GC samples were divided into two clusters based on their distinct clinicopathological features, prognosis, and immune characteristics. Using LASSO and Cox regression analyses, 9 genes were identified for constructing a prognostic signature related to cuproptosis. The novel signature displayed outstanding durability and prognostic capability for the overall lifespan of individuals. Additionally, the expression levels of signature genes in GC tissues and adjacent normal tissues were tested by qRT-PCR. Moreover, we developed a remarkably dependable nomogram to enhance the practicality of the CRG_score in clinical settings. High tumor mutation burden, increased microsatellite instability-high, immune activation, along with good survival probability and increased immunoreactivity to immune checkpoint inhibitors, were distinguishing features of low CRG_scores.
Conclusions: The findings of this study revealed the possible impacts of CRGs on the TME, clinical and pathological characteristics, and outlook of patients with GC. This signature was strongly linked to the immune response against GC and has the potential to serve as a valuable tool for predicting patient prognosis.

* Corresponding author. Department of Gastroenterological Surgery II, Renmin Hospital of Wuhan University, No. 238, Jiefang Road, Wuhan, 430060, China.
E-mail address: liuyanliang828@whu.edu.cn (Y. Liu).
[1] Authors contributed equally to this work.

1. Introduction

Gastric cancer (GC) is a globally prevalent and deadly malignancy characterized by its diverse nature and aggressive behavior. According to the 2020 Global Cancer Report, GC has emerged as the sixth most commonly diagnosed cancer and is the third leading contributor to cancer-related deaths. Consequently, it represents a significant global health emergency [1]. Clinically, GC is primarily managed through surgical removal, chemotherapy, radiation therapy, targeted therapy, or a combination of these approaches. Despite these challenges, patients continue to encounter numerous life-threatening problems, such as relapse, spread of cancer, resistance to medication, absence of suitable drug targets, and adverse reactions. The outcome for patients with GC remains extremely unfavorable, especially for those in advanced stages, where the five-year survival rate is quite low [2]. Despite having similar tumor grading and identical pathological staging, the survival outcomes of patients with GC can vary significantly owing to distinct genetic characteristics. Therefore, identifying new predictive biomarkers and clinical treatment approaches is imperative to enhance the survival and cure of patients with GC.

Cuproptosis, a newly identified form of cellular death, differs from commonly recognized forms of programmed cell death, such as apoptosis, pyroptosis, ferroptosis, and necroptosis [3–5]. Copper (Cu) is an essential trace element in organisms and is involved in cellular processes, such as mitochondrial respiration, kinase signaling, autophagy, antioxidant defense, and redox signaling [6]. Cuproptosis is dependent on the accumulation of copper in vivo. Excess copper binds directly to the lipoylated components of the tricarboxylic acid cycle, promoting the abnormal aggregation of lipoylated proteins and the loss of iron-sulfur cluster proteins. This process may lead to proteotoxic stress and eventual cell death [7]. Mounting evidence indicates that cuproptosis plays a crucial role in both normal and abnormal biological processes involved in various types of cancers. Both carriers of copper ions and substances that bind to copper ions exhibit strong anti-cancer properties [8]. Increased copper concentrations have been observed in tumor tissues and sera of patients with multiple cancer types [9–11]. The dynamic balance of copper plays a vital role in tumorigenesis. However, owing to technical limitations, most studies have been limited to one or two cuproptosis-related genes (CRGs), and the antitumor effects are characterized by many tumor suppressors interacting in a highly coordinated manner. Cancer is currently a very important topic in medicine. Various factors, such as different types of viruses and congenital genetic defects, can play a role in the development of various types of cancers. This underscores the need for conducting studies in the field of cancer [12–15]. Therefore, a comprehensive understanding of various CRG-mediated tumor microenvironment (TME) cell infiltration characteristics will enhance our understanding of TME immune regulation. In this study, we systematically investigated the expression patterns of CRGs and their roles in the clinical outcomes, TME infiltration, tumor mutational burden (TMB), microsatellite instability (MSI) status, and responses to treatments in GC.

2. Materials and methods

2.1. Multi-omics data collection and processing

The TCGA-STAD program was utilized to obtain RNA expression data, somatic mutation data, copy number variation (CNV) files, and clinical data for GC. Additionally, four Gene Expression Omnibus (GEO) datasets (GSE84437, GSE62254, GSE34942, and GSE15459) were merged for further analysis and their batch effects were removed using the "SVA" R package. For the TCGA cohort, the FPKM value was transformed into transcripts per kilobase million (TPM).

A total of 1374 patients with GC were included after excluding those without clinical data, repeated data, incomplete clinical information, and survival time of 0 days. The detailed clinical information is provided in Supplementary Table 1.

2.2. Unsupervised clustering of CRGs

Thirteen CRGs used in this study were obtained from the previous literature [7] and are listed in Supplementary Table 2. The k-means algorithm was employed for consensus clustering to determine unique patterns related to cuproptosis. The number of clusters and their stability were determined using the R package "ConsensuClusterPlus." To ensure classification stability, 1000 iterations were performed [16]. The effect of clustering was evaluated by principal component analysis (PCA) using the R package "stats." To investigate the clinical significance of the molecular subtypes, we assessed the correlation between molecular subtypes, clinical characteristics, and survival outcomes. Moreover, Kaplan–Meier analysis based on the survival and survminer packages was used to evaluate Overall survival (OS) differences between different subtypes.

2.3. Correlation between molecular subtypes and TME in GC

Using the ESTIMATE algorithm, the proportions of different infiltrating stromal and immune cells were deduced from the transcriptome profile of the GC tissues [17]. Subsequently, the presence of 23 immune cell-infiltrating fractions was determined using a gene set enrichment analysis algorithm, which was performed on a single sample.

2.4. Gene set variation analysis

Gene set variation analysis (GSVA) is typically employed to assess the variability in the activity of pathways and biological

processes within samples of expression datasets. The "GSVA" R package was employed to elucidate the variances in biological mechanisms between the two subcategories [18]. To perform GSVA, the gene sets from the MSigDB database (http://software. broadinstitute.org/gsea/msigdb/index.jsp) named "c2.cp.kegg.v7.4. symbols.gmt" were downloaded. The "pheatmap" R package was used to create heat maps.

2.5. Detection of differentially expressed genes and analysis of functional enrichment

To detect differentially expressed genes (DEGs) between various CRG subtypes, we employed the "limma" package [19], applying the following criteria: |fold change (FC)| $\geq$ 1.5 and p-value <0.05. The R package "clusterProfiler" [20] was used to analyze the DEGs in GO and KEGG, employing a cutoff value of an adjusted p-value of <0.05.

2.6. Identification of cuproptosis gene subtypes in GC

The CRG subtype-related DEGs associated with OS in patients with GC were selected using univariate Cox regression analysis. Subsequently, we conducted consensus clustering using the "ConsensusClusterPlus" R package to screen distinct CRG subtypes. Kaplan–Meier analysis was then conducted to analyze the differences in OS. Moreover, we analyzed the correlation between the different gene subtypes and clinical traits.

2.7. Construction and validation of prognostic signature

For an in-depth investigation of the prognostic prediction potency of DEGs in GC cases, all patients in GEO were randomly assigned to a training cohort or a testing cohort at a 7:3 ratio. The training cohort was used to construct the prognostic signature; meanwhile, the test and TCGA cohorts were used as internal and external validation cohorts, respectively, to validate the predictive accuracy of the signature. To avoid overfitting, LASSO regression analysis using 10-fold cross-validation was conducted on the training cohort [21]. Subsequently, a prognostic model (the CRG_score) was established using multivariate Cox analysis. The CRG_score was calculated using the following formula:

$$\text{CRG\_score} = \sum_{i=1}^{n} Coefi \times Expi$$

here, Coef and Exp refer to the regression coefficient and gene expression, respectively. All patients with GC were equally stratified into low- and high-risk categories based on the computed median CRG_score. The differences in survival probability among distinct groups were compared using Kaplan–Meier analysis. Receiver operating characteristic (ROC) curves were constructed to explore the predictive ability of the CRG_score. PCA was conducted to differentiate the patients with GC into two risk groups.

The internal and external validation cohorts were utilized to confirm the prognostic signatures associated with cuproptosis. The training cohort stratified the patients into two risk subgroups using the CRG_score cut-off point. Kaplan–Meier survival plots were created to assess the disparities between the two risk categories. Similarly, the validity of the prognostic signature was evaluated using ROC curves and PCA.

2.8. Analysis of the prognostic CRG_score's clinical significance and classification

An investigation was conducted to examine the correlation between the CRG_score and clinical variables (tumor location, Lauren classification, sex, age, and TNM stage). Univariate and multivariate Cox regression analyses were conducted to determine whether the CRG_score acted as a standalone prognostic predictor. Next, a classification analysis was conducted to investigate whether the CRG_score maintained its predictive accuracy in various subgroups defined by different clinical variables.

2.9. Establishment of nomogram and calibration

A graphical representation, known as a nomogram, was created to offer significant clinical forecasts for patients with GC. It was created based on their risk scores and various clinicopathological features, specifically focusing on the OS rates at one, three, and five years. Each variable in the nomogram was assigned a score and the total score for each sample was calculated by summing up the scores of all variables. ROC curves were used to evaluate the performance of the nomogram in predicting the survival rates at 1, 3, and 5 years. Calibration plots of the nomogram were used to depict the prognostic significance of the expected survival outcomes at 1, 3, and 5 years in comparison to the observed outcomes.

2.10. Estimation of immune infiltration status and immunotherapeutic response

The CIBERSORT algorithm was employed to examine the abundance of 22 immune cells [22]. The Wilcoxon signed-rank test was used to analyze the distinct compositions of immune-infiltrating cells in the two risk groups. The results were then visualized using a box chart. Upon further examination, we demonstrated the associations between the prevalence of immune cells and nine model genes. The correlation between the CRG_score and TME score was studied using the ESTIMATE algorithm. To assess the patient's reaction to immunotherapy, the "ggpubr" R packages were utilized to assess whether immune checkpoint activation differs between different risk

groups. Furthermore, we acquired tumor immune dysfunction and exclusion (TIDE) scores from the Internet (http://tide.dfci.harvard.edu/) [23]. TIDE scores can predict the response of low- and high-risk patients to PD-1 and CTLA4 immune checkpoint response inhibitors. These scores can help physicians select patients who are more suitable for immune checkpoint therapy. Subsequently, we employed the immunophenoscore (IPS) to predict the efficacy of ICIs by analyzing the expression of the primary element in tumor immunity. When the IPS is higher, the response to immunotherapy is generally better [24]. The patients with GC were obtained from The Cancer Immunome Atlas website (https://tcia.at/).

2.11. Analysis of tumor mutation burden and microsatellite instability

The gene mutation in various risk subgroups was analyzed using the "maftools" R package [25]. Furthermore, we investigated the correlation between the CRG_score and TMB. The function surv_cutpoint from the R package "survminer" was used to determine the ideal threshold for TMB in survival data. Subsequently, patients were categorized into subgroups based on low and high TMB levels. To compare the OS of patients with GC between the two groups, the Kaplan–Meier method was utilized. Subsequently, an integrated examination of TMB and CRG scores was conducted to investigate variations in OS among distinct cohorts. Furthermore, the relationship between CRG_scores and MSI was investigated.

2.12. Evaluation of drug responsiveness

The patients were divided into two CRG_score subgroups to predict their responsiveness to different medications. The "oncopredict" R package was developed by Maeser et al. [26] to predict drug responses in patients with cancer. In total, 198 drugs were evaluated, and the disparity in half inhibitory concentration (IC50) values among various risk subgroups was examined using the Wilcoxon signed-rank test.
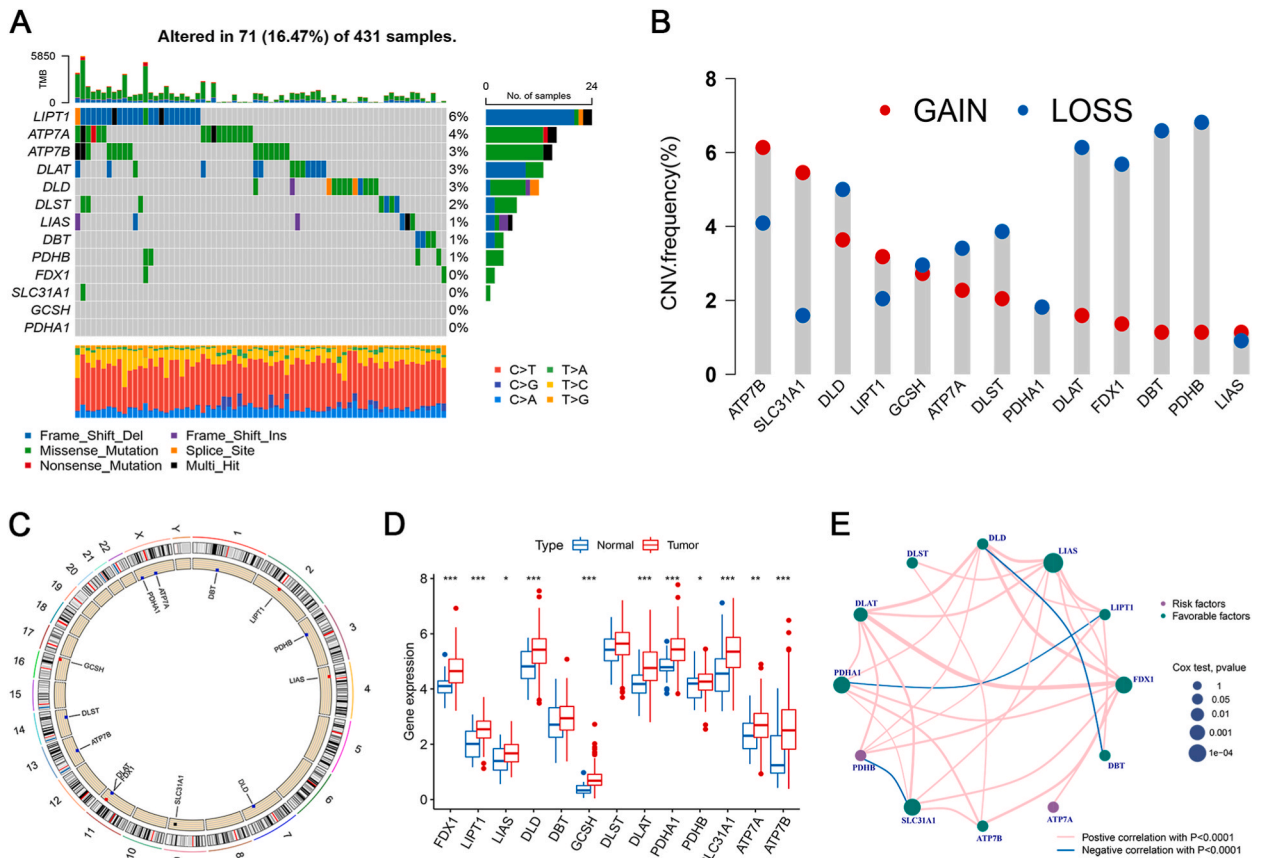

Fig. 1. Changes in the genetic and transcriptional profiles of CRGs in GC. (A) Mutation frequency of 13 CRGs in GC patients in the TCGA-STAD cohort. (B) Frequencies of copy number variation (CNV) of 13 CRGs in GC. (C) Chromosome distributions of CRGs are depicted in circus plots. (D) The expression distributions of 13 CRGs in GC and normal gastric tissues. (E) Interaction among CRGs in GC. The interaction among CRGs is depicted by the connecting line, with the thickness of the lines indicating the strength of their association. Negative and positive correlations are represented by blue and pink, respectively. The significance levels are denoted as follows: $p < 0.05$ (*), $p < 0.01$ (**), and $p < 0.001$ (***).

2.13. Tissue sample collection and qRT-PCR

The tissue samples used in this study were collected from the Gastrointestinal Surgery Department of Renmin Hospital, Wuhan University. The study was approved by the Ethics Committee of the Hospital, and written informed consent was obtained from the patients and participants. Three pairs of GC tissues and their corresponding tissues were collected from patients with GC. All samples were maintained at −80 °C.

Total RNA was extracted from tissues using the TRIzol reagent (Invitrogen; Thermo Fisher Scientific, Inc.) following the manufacturer's instructions. cDNA was synthesized using a RevertAid First Strand cDNA Synthesis Kit (K1622; Thermo, USA). For real-time
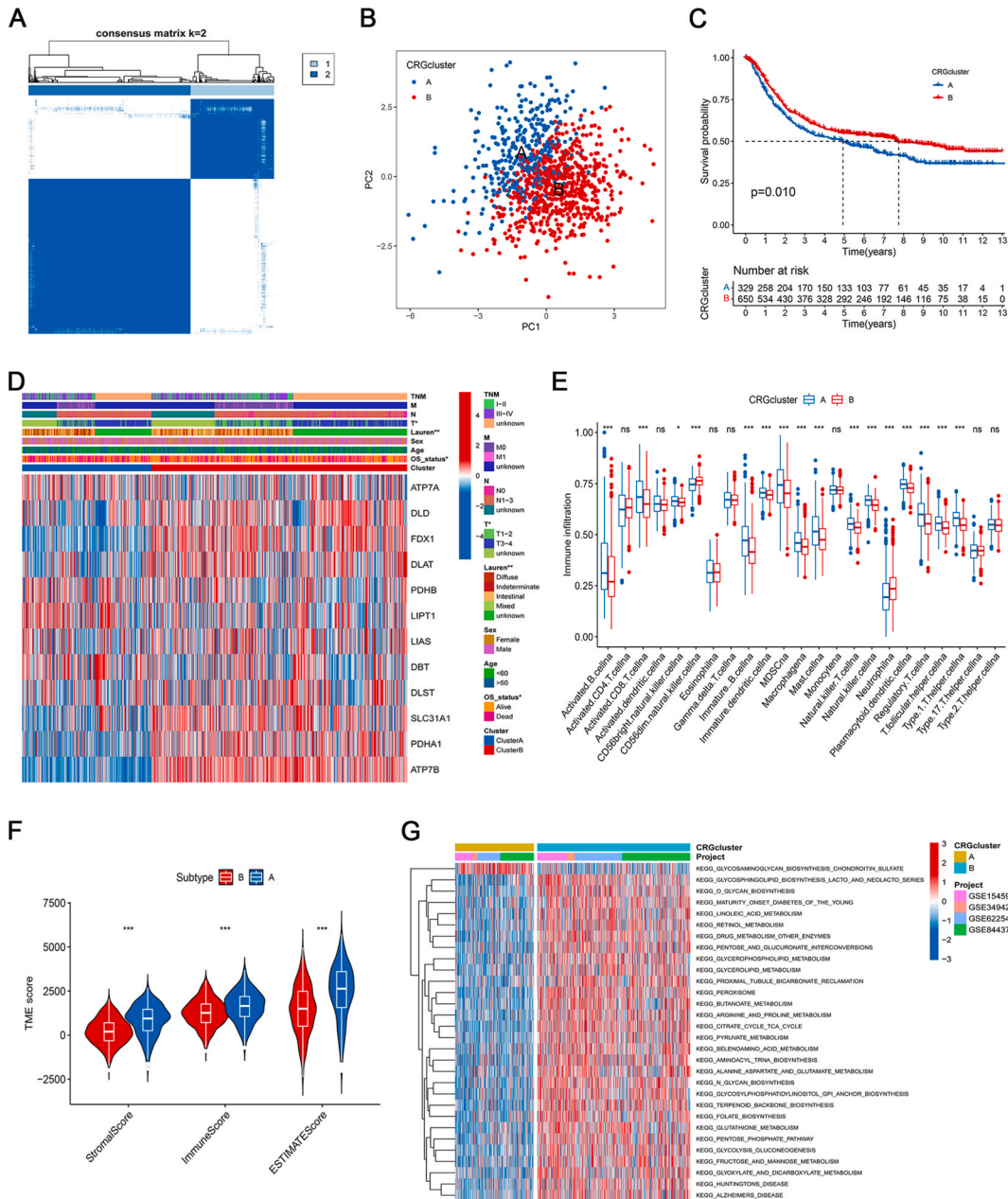

Fig. 2. Characteristics of TME and biological function in different CRG subtypes. (A) The heatmap of the consensus matrix delineates two clusters (k = 2) and their corresponding correlation region. (B) PCA showed significant differences among the two subtypes. (C) Kaplan-Meier curves for survival differences among the two subtypes. (D) The heat map presented the distribution of the clinicopathological traits and the differential expression of 12 CRGs between two subtypes. (E) Differences in infiltration abundance of 23 immunocytes among the two CRG subtypes. (F) Correlations observed between the TME score and the two GC subtypes. (G) Calculation of GSVA for biological pathways in two different subtypes. The significance levels are denoted as follows: $p < 0.05$ (*), $p < 0.01$ (**), and $p < 0.001$ (***).
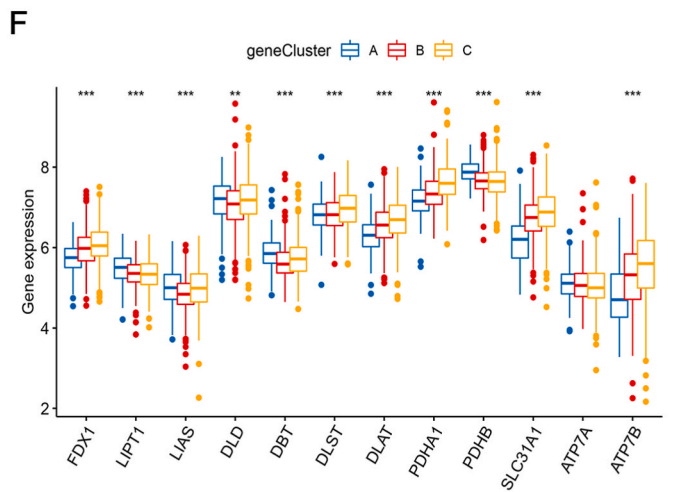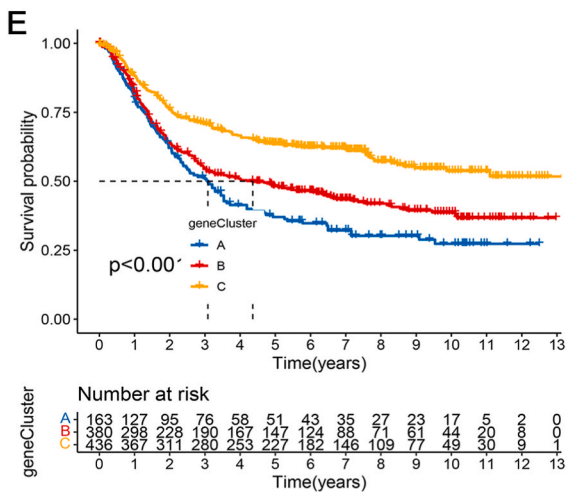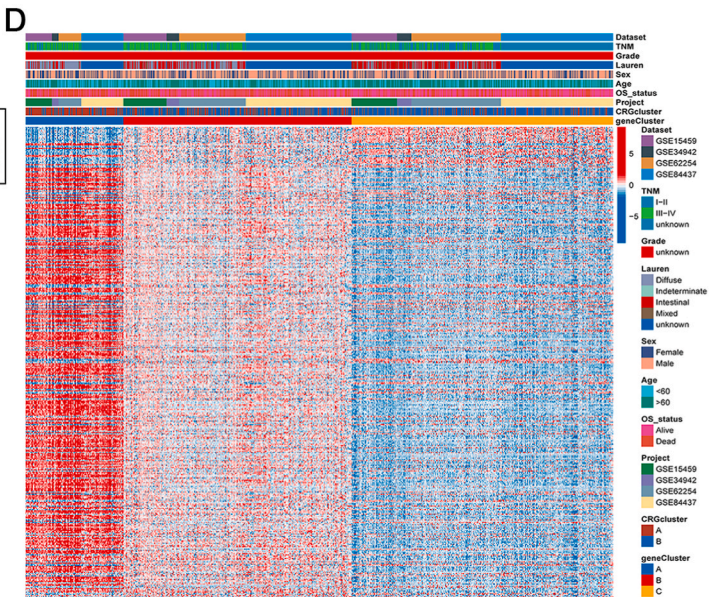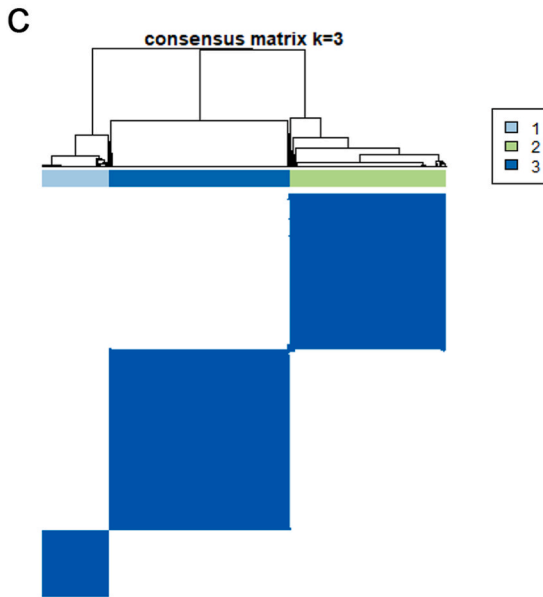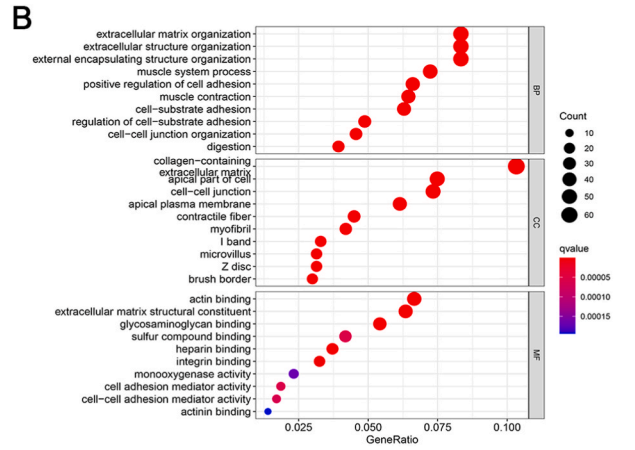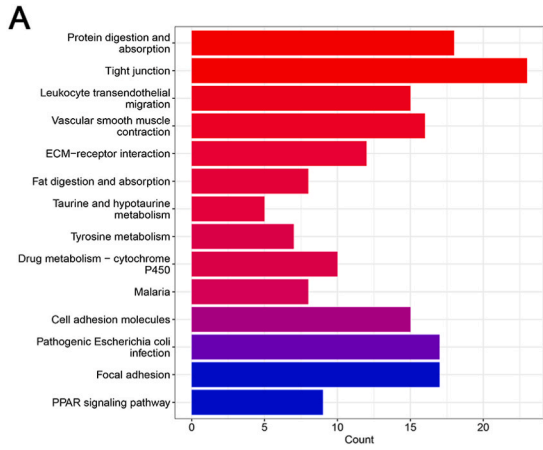
(caption on next page)

Fig. 3. Classification of gene subcategories using DEGs. (A) KEGG pathway of DEGs within three genetic subtypes. (B) GO enrichment analyses on DEGs within three genetic subtypes. (C) GC patients were grouped into three genotypes. (D) The correlation between clinicopathologic characteristics and the three genetic subtypes. (E) Kaplan-Meier plots illustrating overall survival (OS) for the three genetic subtypes. (F) Divergences in the manifestation of CRGs across the three genetic subtypes. The significance levels are denoted as follows: $p < 0.05$ (*), $p < 0.01$ (**), and $p < 0.001$ (***).

PCR analysis, all PCRs were performed using the HieffTM qPCR SYBR® Green Master Mix (No Rox Plus) (11201 ES; Yeasen Bio-Technologies, China). Gene expression was measured using CFX-96 qPCR platform (Bio-Rad Laboratories, Inc., USA). The fold changes were calculated with the $2^{-\Delta\Delta Ct}$ method, with GAPDH as the internal control. Primer sequences are listed in Supplementary Table 3.

2.14. Statistical analysis

The data were processed, analyzed, and presented using the R software (version 4.2.0) and its corresponding R packages. A two-tailed P-value <0.05 was considered significant. Differences between non-parametric and parametric methods were evaluated using the Wilcoxon or Kruskal-Wallis test. The Spearman's correlation test was used to compute the correlation coefficients. The survival prognosis was analyzed using the Kaplan–Meier test, and variations between the groups were evaluated using the log-rank test. Hazard ratios (HR) for CRGs were calculated using univariate Cox regression analysis. To determine whether the CRG_score was a separate prognostic indicator, we included both the CRG_score and the related clinicopathological traits in an analysis using a multivariate Cox regression model.

3. Results

3.1. The landscape of genetic alterations and variations in the expression of CRGs in patients with GC

In the TCGA cohort, we examined genetic alterations to comprehend the various mutation categories of the chosen CRGs in GC specimens (Fig. 1A). Approximately 16.47% of the 431 samples exhibited CRG mutations at the genetic level. *LIPT1* exhibited the highest mutation frequency among the 13 CRGs, followed by *ATP7A, ATP7B, DLAT, DLD, DLST, LIAS, DBT*, and *PDHB* (Fig. 1A). Next, we analyzed the frequencies of copy number variations (CNV) in the 13 CRGs associated with GC. As shown in Fig. 1B, *ATP7B, SLC31A1*, and *LIPT1* showed an extensively increased CNV, whereas *PDHB, DBT, DLAT, FDX1, PDHA1, ATP7A, DLST*, and *DLD* exhibited an extensively reduced CNV. The locations of CNV alterations in 13 CRGs on 23 chromosomes are presented in Fig. 1C. We further assessed the expression levels of 13 CRGs in tumor and normal samples. Eleven CRGs were highly expressed in the tumor samples compared to the normal samples (Fig. 1D). Fig. 1E illustrates the establishment of a network displaying the complete landscape of interconnections among the chosen CRGs, regulator linkages, and their prognostic importance in patients with GC (Fig. 1E; Supplementary Table 4).

3.2. Identification of cuproptosis clusters

To investigate the correlation between the expression patterns of CRGs and GC subtypes, we employed an unsupervised clustering method. This method detected distinct regulatory patterns by analyzing the expression levels of the 13 CRGs. The classification of the entire group into subcategories A (n = 329) and B (n = 650) indicates that k = 2 was the ideal selection (Fig. 2A and Table S1). Additionally, the excellent intergroup distribution was confirmed by the results of the PCA, as shown in Fig. 2B. The survival analysis indicated that cluster B exhibited a higher likelihood of survival than cluster A ($P = 0.010$; Fig. 2C). Furthermore, Fig. 2D illustrates the comparison of gene expression and clinicopathological variables between the two clusters. This analysis revealed a significant disparity in the expression of CRGs and clinical characteristics.

3.3. Characteristics of TME and biological function in different CRG subtypes

To determine the correlation between CRGs and the TME of GC, we investigated the infiltration levels of 23 different immune cell subpopulations of the two CRG clusters. Fig. 2E illustrates a significant disparity in immune cell enrichment between the two clusters. In cluster A, the levels of activated B cells, immature B cells, CD56 (bright) natural killer (NK) cells, NK cells, activated CD8 T cells, NK T cells, T follicular helper (Tfh) cells, immature dendritic cells (DC), plasmacytoid DC, macrophages, MDSC, mast cells, Tregs, and Th1 cells were significantly higher than those in cluster B; whereas, CD56 (dim) NK cells and neutrophils exhibited the opposite trend. Furthermore, by utilizing the ESTIMATE algorithm, we calculated the TME scores for various subtypes, which encompassed the stromal, immune, and estimated scores. Using these scores, we assessed the abundance of immune and stromal elements in the TME. The results showed that individuals in the cluster A exhibited elevated TME scores compared to those in the cluster B (Fig. 2F).

The results of the GSVA analysis revealed that cluster B exhibited a high number of pathways related to metabolic activation (such as linoleic acid metabolism, retinol metabolism, and glycerophospholipid metabolism) (Fig. 2G; Supplementary Table 5).

3.4. Identification of gene subgroups based on DEGs

To examine the inherent biological function of CRG subtypes, we acquired 678 DEGs associated with CRG subtypes by utilizing the "limma" package and performed functional enrichment analysis. KEGG analysis indicated an abundance of pathways associated with metabolic processes, such as taurine and hypotaurine metabolism, tyrosine metabolism, and metabolism-cytochrome *P*450, which were consistent with the results of GSVA (Fig. 3A). Furthermore, GO pathway analysis indicated enrichment in the organization of the extracellular matrix (ECM), ECM containing collagen, and structural constituents of the ECM (Fig. 3B). These findings indicate that cuproptosis might play a vital role in tumorigenesis and GC development.

Next, we conducted an uniCox analysis to assess the survival importance of 678 CRG subtype-related DEGs, resulting in the identification of 365 genes meeting the criteria of $P < 0.05$ (Supplementary Table 6; $P < 0.01$). To examine this regulatory mechanism, a consensus clustering method was employed to categorize the individuals into three gene clusters (clusters A–C) (Fig. 3C). As expected, there were obvious differences in the clinicopathological traits among the three gene classifications (Fig. 3D). Based on the Kaplan–Meier curves, cluster A patients had the shortest OS duration, whereas patients of cluster C experienced a higher OS time (Fig. 3E, $P < 0.001$). As observed from the patterns (Figs. 3F), 11 of the 12 CRGs exhibited notable variations among the three gene subcategories.

3.5. Generation and verification of the prognostic CRG_score

The CRG_score was developed using the subtype-related DEGs. A total of 979 patients with GC were randomly assigned to either the training group (n = 687) or the test group (n = 292) at a 7:3 ratio. After LASSO regression analysis, 10 genes associated with the OS of patients were identified based on the least partial likelihood of deviance (Fig. 4A and B). Subsequently, a multivariate Cox regression analysis was conducted, resulting in the identification of 9 genes (*FLNA, COL8A1, MKX, SGCE, PTGIS, ASCL2, CDC42EP5, e*, and *CXCL13*), for the development of the prognostic model called the "CRG_score" (Fig. 4C).

3.6. The coefficients of 9 genes were used to calculate the CRG_score

CRG_score = (0.2816 × FLNAexp) + (0.3400 × COL8A1exp) + (−0.2993 × MKXexp) + (0.3080 × SGCEexp) + (−0.2937 × PTGISexp) + (−0.0783 × ASCL2exp) + (−0.1136 × CDC42EP5exp) + (0.1176 × COMPexp) + (−0.1119 × CXCL13exp).

The computed median CRG_score was used to differentiate between high- and low-risk subcategories. The PCA results indicated that patients with GC could be separated into two subtypes (Fig. 5A). Survival analysis demonstrated that low-risk patients exhibited superior OS, CSS, and PFS compared with high-risk patients (Fig. 5B–D). Fig. 5E shows that, as the CRG_score increased, the distribution plot indicated a decrease in survival time (Fig. 5E). Furthermore, we generated ROC curves for survival over one, three, and five years and determined that the corresponding AUC values were 0.765, 0.794, and 0.786, respectively (Fig. 5F). A significant variation in the CRG_score was observed between the CRG subtypes and gene subtypes (Fig. 5G and H). The CRG_scores of subtype A were higher than those of subtype B (Fig. 5G). Gene cluster A had the highest CRG_score, whereas gene cluster C had the lowest CRG_score. (Fig. 5H). Fig. 5I illustrates the breakdown of patients across the two CRG subtypes, three gene subtypes, and two groups based on the CRG_score.

To assess the reliability of the CRG_score in making predictions, we obtained the CRG_scores for both the internal (testing cohort) and external (TCGA cohort) datasets. Patients were classified into two risk subcategories based on the median score of the training cohort. Using PCA, patients with different risks were categorized into two distinct clusters (Fig. 6A and B). Similarly, the examination of patient survival indicated that individuals classified as low-risk experienced superior OS compared with those classified as high-risk (Fig. 6C and D). Compared to the low CRG_score subgroup, a higher number of death events and shorter OS times were observed in the
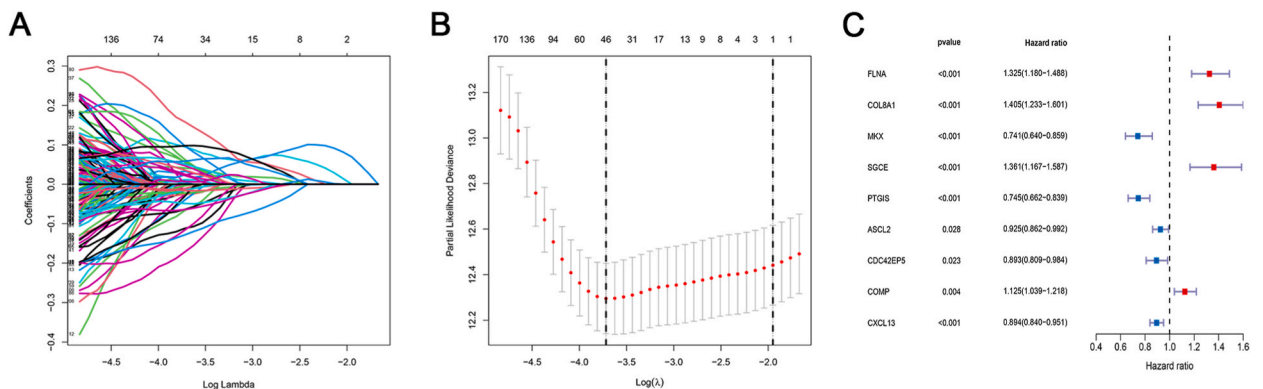

Fig. 4. Identification of prognostic cuproptosis-related genes in GC patients. (A) The LASSO coefficient spectrum of the 46 OS-related genes. (B) Cross-validation for tuning parameter selection in the LASSO analysis. (C) Multivariate Cox regression analysis of the 9 genes for the OS of GC patients.
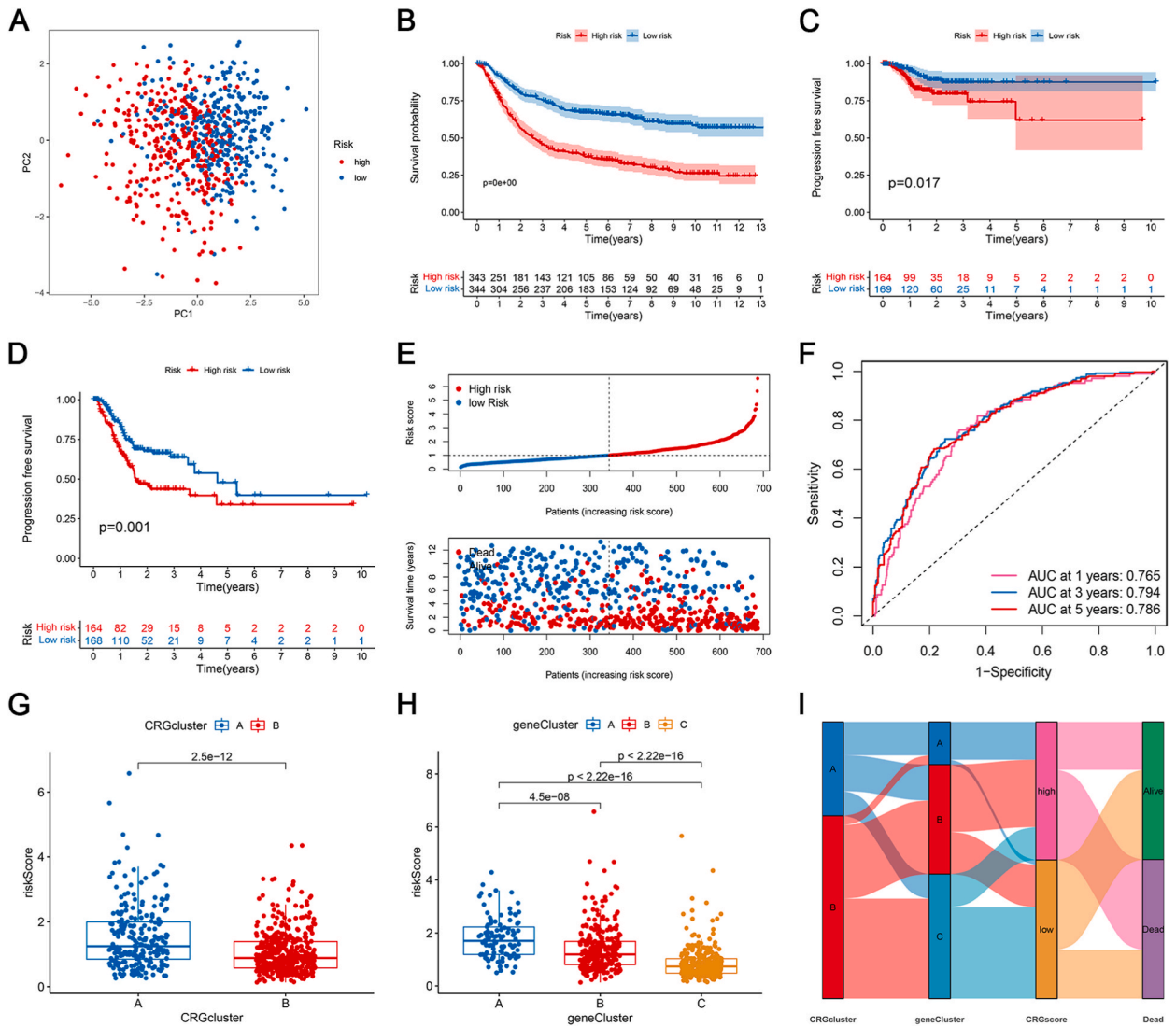
Fig. 5. Construction and verification of CRG_score in the training cohort. (A) Principal Component Analysis showing the distribution of CRG_score and patient survival status through ranked dot and scatter plots. (B–D) Kaplan-Meier survival analysis of OS (B), CSS (C), and PFS (D) for GC patients with low- and high-risk groups. (E) Dot and scatter plots were used to rank the distribution of CRG_scores and patient survival status. (F) ROC curves are used to forecast the sensitivity and specificity of survival for 1, 3, and 5 years based on the CRG_score. (G) Divergences in CRG_score among two CRG subtypes. (H) Divergences in CRG_score among the three gene subtypes. (I) An alluvial diagram illustrating the distribution of subtypes in various groups based on different CRG_scores and their corresponding survival outcomes.

high CRG _ score subgroup (Fig. 6E and F). The forecast of the likelihood of survival at one, three, and five years indicated that the CRG_score continued to exhibit impressive AUC values, indicating its robust capability to assess the outcome of individuals with GC (Fig. 6G and H).

3.7. Clinical value of the prognostic CRG_score

To investigate the clinical significance of the prognostic CRG_score, we performed a correlation analysis. As illustrated in Fig. 7A–D, the CRG_score was associated with T, N, TNM stage, and Lauren classification (Fig. 7A–D). The CRG_score was higher in patients with T 3–4, N 1–3, and TNM stages (Fig. 7A–C), and a significantly higher CRG_score was obtained for patients with diffuse-type GC than for patients with intestinal-type GC (Fig. 7D). To explore the predictive importance of the CRG_scores, patients with GC were categorized into various subgroups according to their clinical factors (Fig. 8). Compared to high-risk patients with GC, low-risk patients showed superior OS in subclasses categorized by the Lauren classification (Fig. 8A–C), location (Fig. 8D and E), clinical stage (Fig. 8F and G), age (Fig. 8H and I), sex (Fig. 8J, K), T stage (Fig. 8L, M), and N stage (Fig. 8N and O) (all $P < 0.05$). This result suggest that the signature was closely correlated with multiple clinical traits. In other words, a higher CRG_score was linked to a more harmful clinical
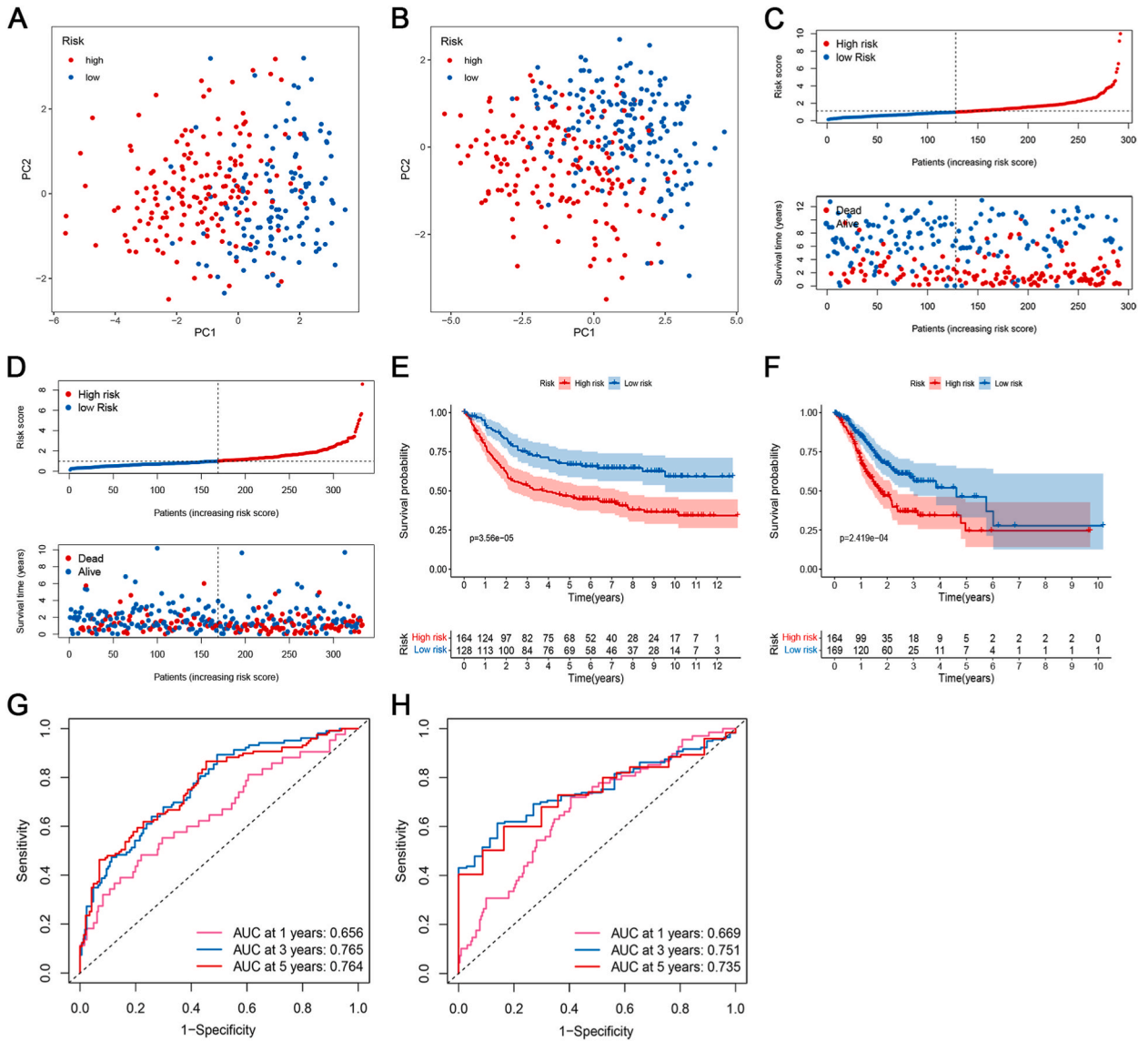
Fig. 6. Validation of the cuproptosis-related signature in the testing and TCGA cohorts. (A, B) GC patients in distinct risk groups could be separated into two subtypes by the PCA in the testing cohort (A) and TCGA cohort (B). (C, D) Distribution of CRG_score and survival status of GC patients in the testing cohort (C) and TCGA cohort (D). (E, F) Kaplan-Meier survival analysis of overall survival (OS) for GC patients with low- and high-risk groups in the testing cohort (E) and TCGA cohort (F). (G, H) Time-dependent ROC analysis in the testing cohort (G) and TCGA cohort (H).

condition. Univariate and multivariate analyses were conducted to investigate the prognostic autonomy of various clinical factors. Fig. 7E shows that age, location, CRG_score, and T and N stages were remarkably correlated with GC prognosis in univariate Cox analysis. Following additional multivariate Cox regression analysis, Fig. 7F demonstrates that the CRG_score emerged as a distinct prognostic determinant after adjustment for various clinicopathologic factors.

To enhance the clinical usefulness of the CRG_score in predicting OS in patients with GC, a nomogram was created that integrates the CRG_score and clinicopathological features to estimate OS rates at 1, 3, and 5 years (Fig. 7G). The AUC values of these clinical variables were computed to predict OS at 1, 3, and 5 years. The AUC values shown in Fig. 7H were as anticipated, indicating that this nomogram demonstrated a remarkable predictive capacity for prognosis. In addition, the calibration curves of the established nomogram showed excellent precision when actual observations were compared with the predicted values (Fig. 7I). These findings indicate that the CRG_scores exhibited a more advanced predictive capability.

3.8. Immune landscape of subgroups based on CRG scores

Using the CIBERSORT algorithm, we evaluated the relationship between the CRG_score and the prevalence of 22 immune cells. As
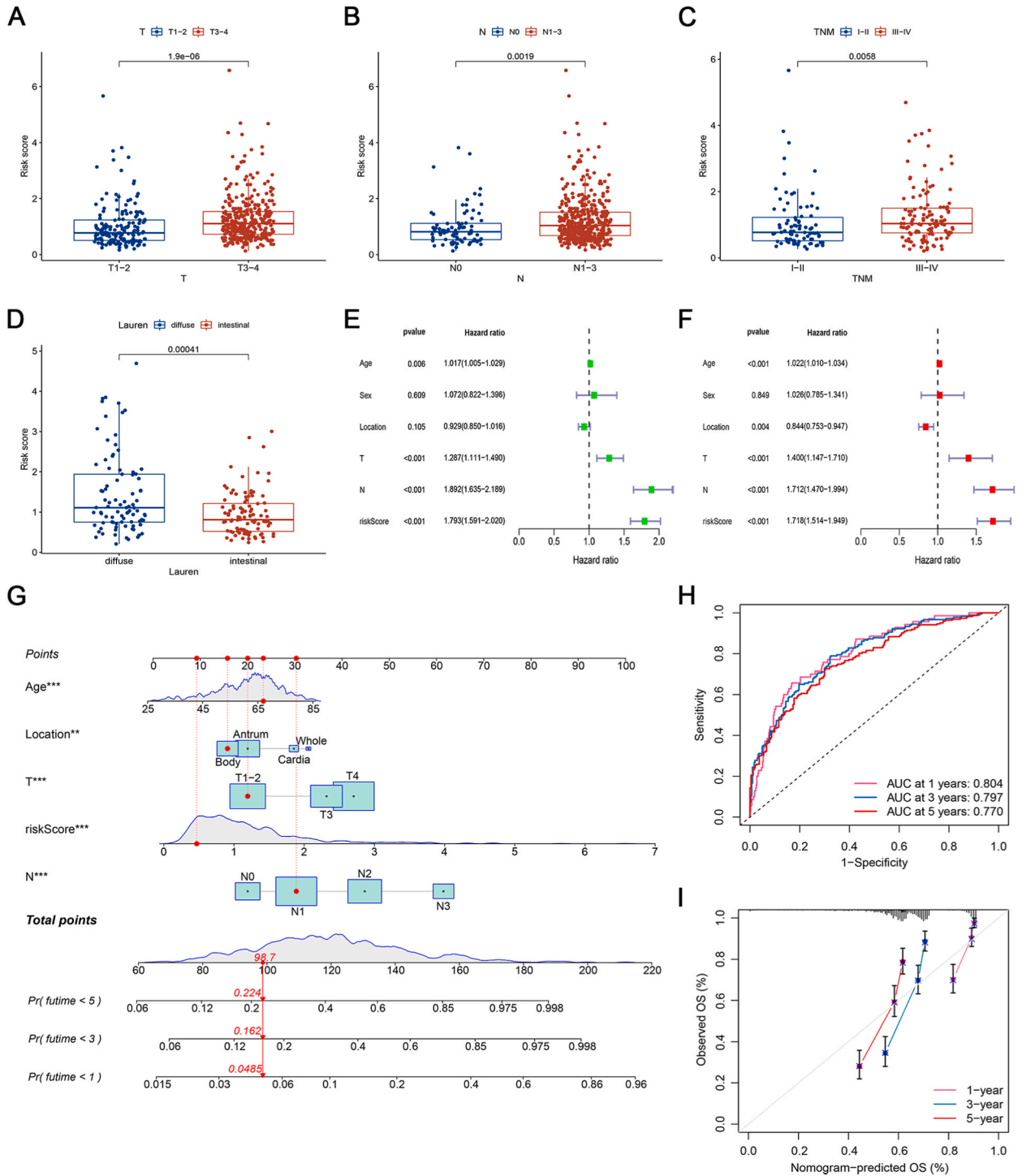
Fig. 7. The clinical value of cuproptosis signature. (A–D) The relationship between the CRG_score and T stage, N stage, TNM stage, and Lauren classification. (E) A univariate Cox regression analysis of CRG_score that significantly influence outcomes in GC. (F) A multivariate Cox regression analysis of CRG_score that significantly influence outcomes in GC. (G) Nomogram is available to predict the OS of GC patients for 1, 3, and 5 years. (H) AUC curves to predict the accuracy of the nomogram. (I) Calibration graphs for the nomogram to predict 1-, 3-, and 5-year OS.

shown in Fig. 9A–D, the CRG_score exhibited a favorable association with the presence of M2 Macrophages, resting memory CD4^{+} T cells, resting mast cells, and monocytes. In contrast, the CRG_score was inversely correlated with activated memory CD4^{+} T cells, CD8^{+} T cells, and M1 Macrophages (Fig. 9E–G). Furthermore, we investigated the ramifications of the CRG_score in the TME of GC tissues
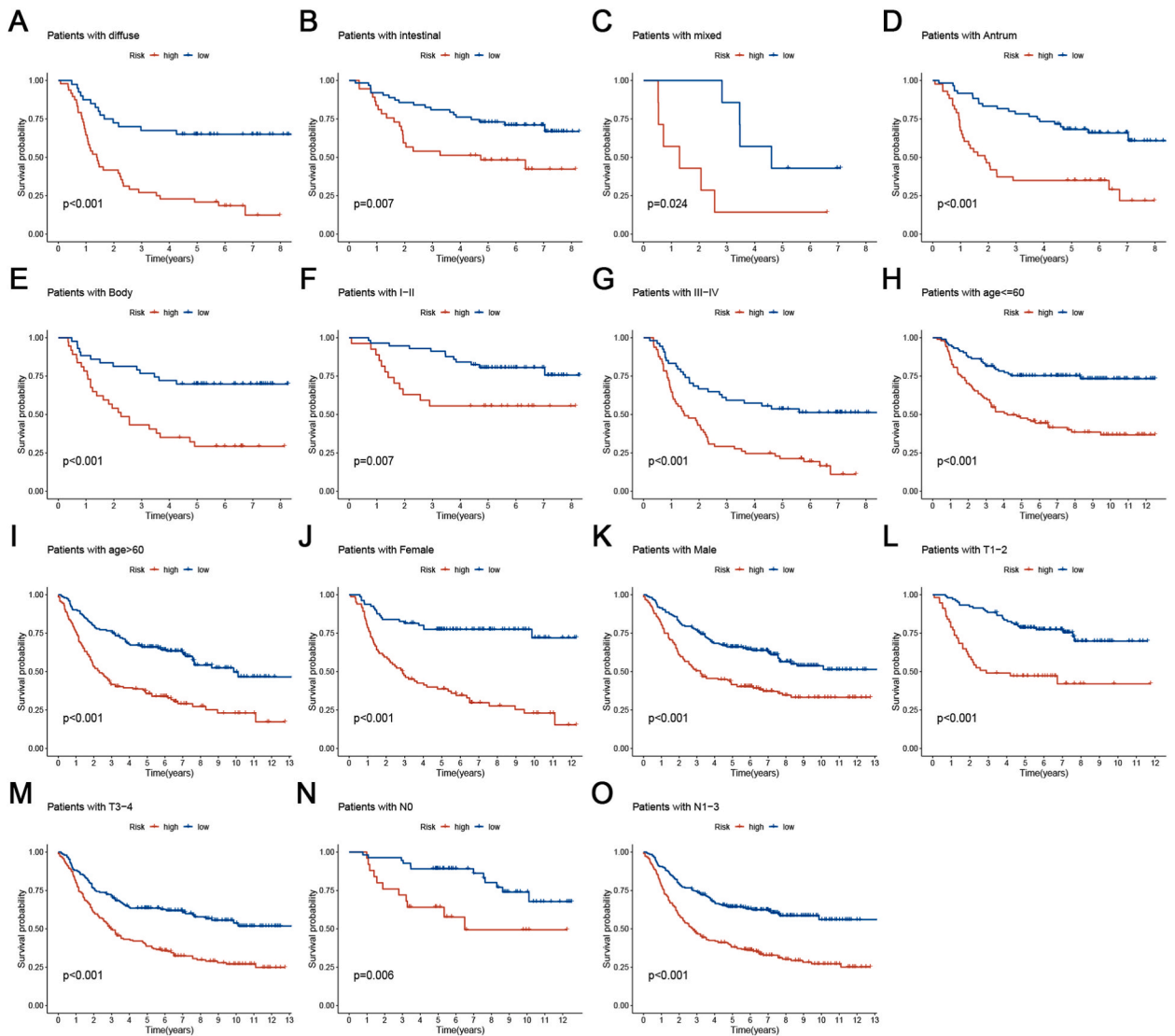
Fig. 8. Clinical stratification analysis of overall survival of patients with GC in the high- and low-risk groups by Lauren classification (A–C), location (D, E), clinical stage (F, G), age (H, I), sex (J, K), T stage (L, M), and N stage (N, O).

using the ESTIMATE algorithm and found that the stromal and ESTIMATE scores were higher in the low-risk subgroup (Fig. 9H). We also evaluated the relationship between infiltrating immune cells and nine signature CRGs and observed that these nine genes were associated with the majority of immune cells (Fig. 9I).

3.9. Analysis of immunotherapeutic responses and drug susceptibility

We compared the expression of common immune checkpoints between the two risk subgroups. The results revealed that the high-risk subgroup samples expressed significantly low levels of PD-1 (PDCD1), PD-L1 (CD274), and CTLA4; conversely, these samples expressed a high levels of CD276, CD44, and CD86 (Fig. 10A). A high TIDE forecast rating correlates with an increased likelihood of immune escape, indicating that patients are unable to benefit from immunotherapy intervention. The low-risk subgroup exhibited decreased TIDE scores compared to the high-risk subgroup, indicating that low-risk patients had a higher likelihood of benefiting from ICI treatment (Fig. 10B). In addition to employing the TIDE score, we examined the association between the risk score and IPS to predict the response to immunotherapy. Our findings revealed a notable increase in the immunogenicity of ICIs in the low-risk group, identified based on the level of risk (Fig. 10C–F). The combined findings demonstrated that the low-risk group had a higher probability of exhibiting an immune response and a positive reaction to immunotherapy.

Finally, we attempted to establish the connections between various risk classifications and the efficacy of chemotherapy in the treatment of GC. We demonstrated that a low IC50 of chemotherapeutics, such as Bortezomib, Dasatinib, and Pazopanib ($P < 0.05$),
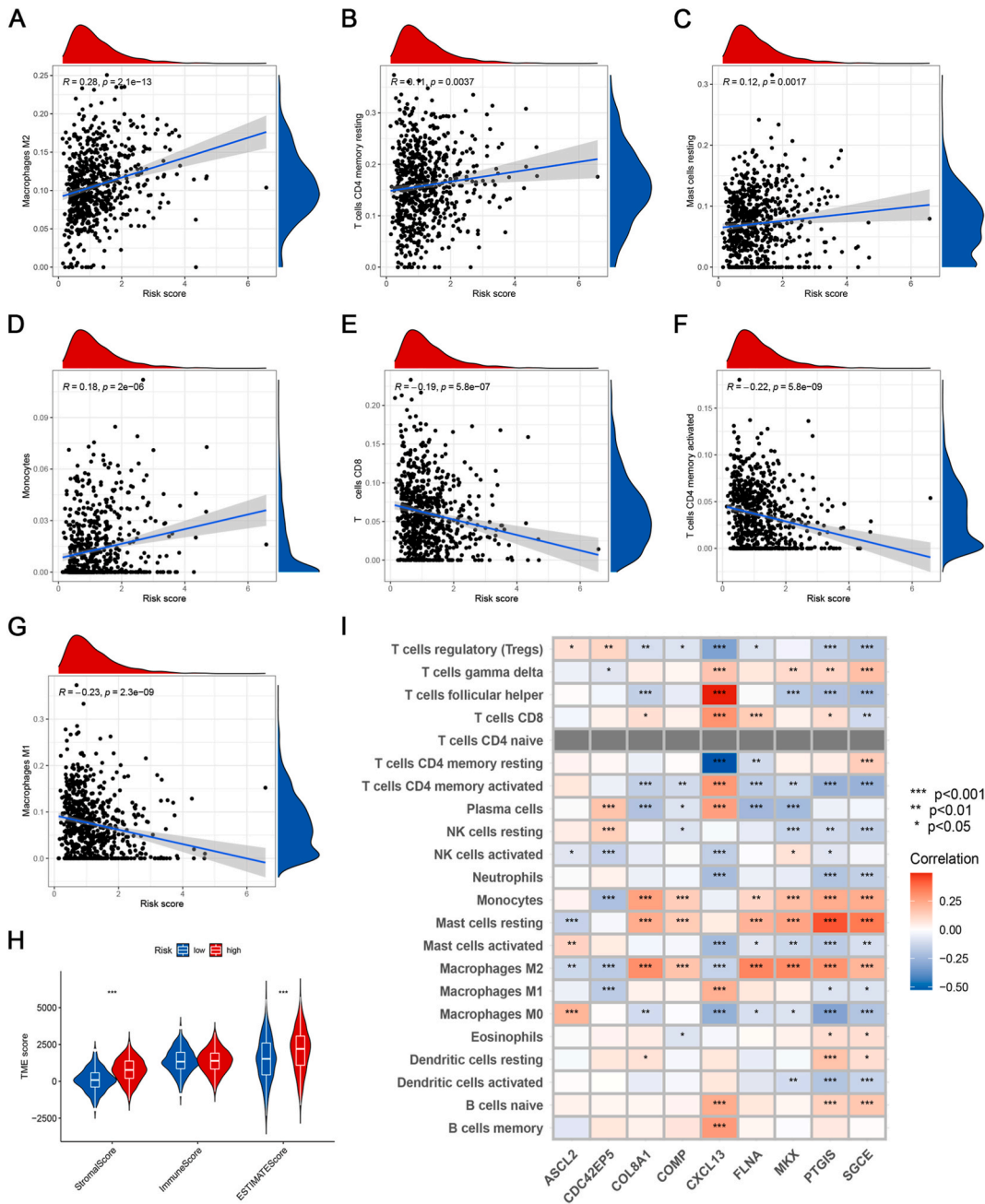
Fig. 9. Immune landscape of the subgroup with CRG scores. (A–G) The relationship between CRG_score and different types of immune cells. (H) Comparison of immune-related scores between two risk subgroups. (I) Correlations observed between the prevalence of immune cells and 9 specific genes in the prognostic model.

was linked to high risk; whereas, a low IC50 of Gefitinib and Metformin ($P < 0.05$) was associated with low risk. Hence, Fig. 10G–K demonstrates that the CRG_score served as a potential indicator of sensitivity to chemotherapy.

3.10. Correlation analysis of CRG_score with TMB and MSI

To gain a deeper understanding of the immunological characteristics of different risk subcategories, we examined variations in the distribution of somatic mutations among different CRG_score groups in TCGA-STAD dataset. We identified 20 genes that exhibited the highest mutation rates in the two risk subgroups (Fig. 11A and B). These findings indicate that missense mutations were the predominant type of mutation. Mutation rates of *TTN*, *TP53*, and *MUC16* were >20% in both groups, indicating their prevalence in both
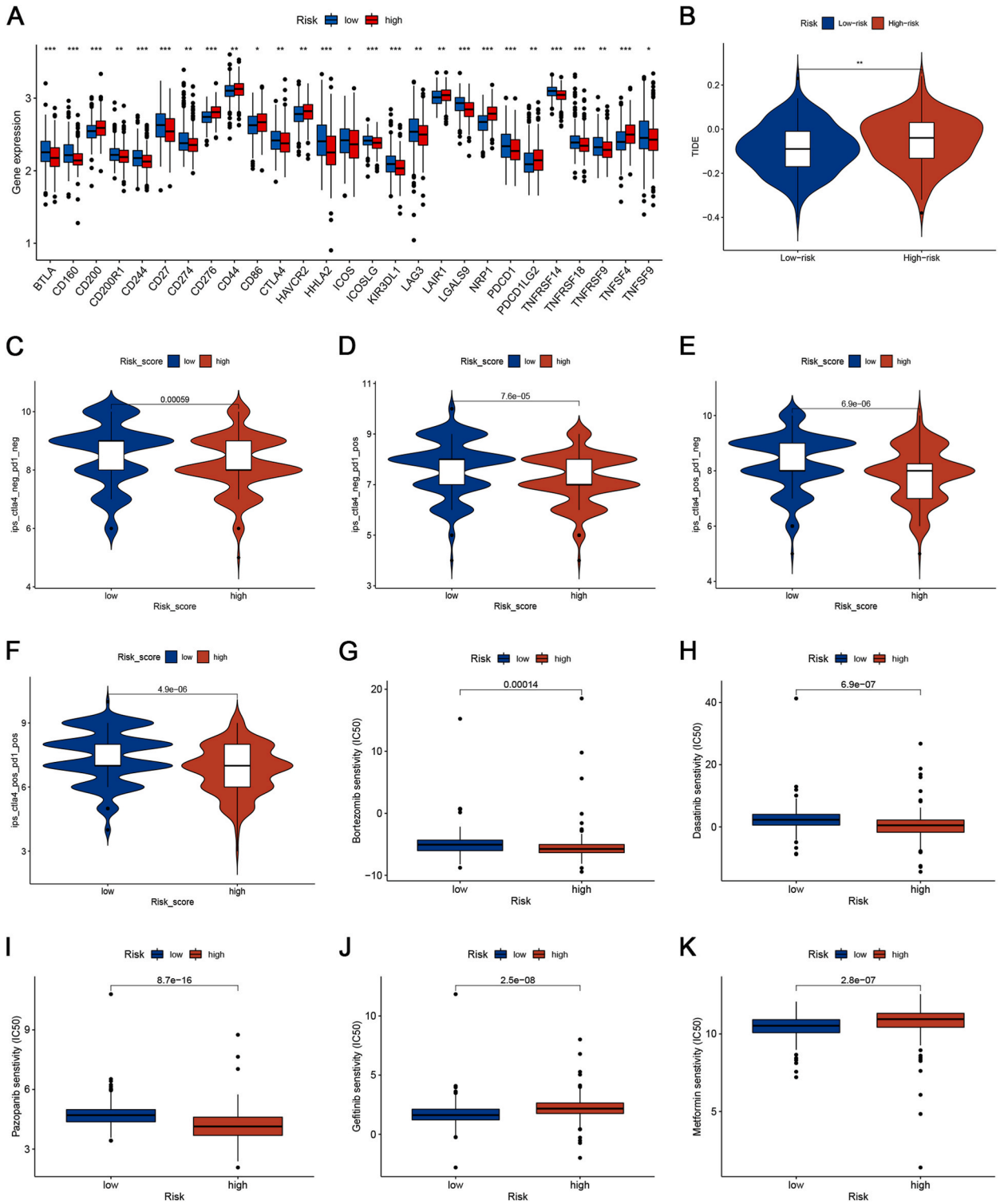
Fig. 10. Analysis of immunotherapeutic responses and drug susceptibility. (A) The boxplot illustrating the variation in expression levels of common immune checkpoints between the high-risk and low-risk groups. (B) The difference of TIDE scores in different CRG_score subgroups. (C–F) Sensitivity analysis of two risk subgroups to immune checkpoint blocking therapy, including anti-PD-1 and anti-CTLA4, or a combination of both. (G–K) The IC50 of the specified chemotherapy drugs was lower in the high (J–I) and low (J–K) CRG_score groups.

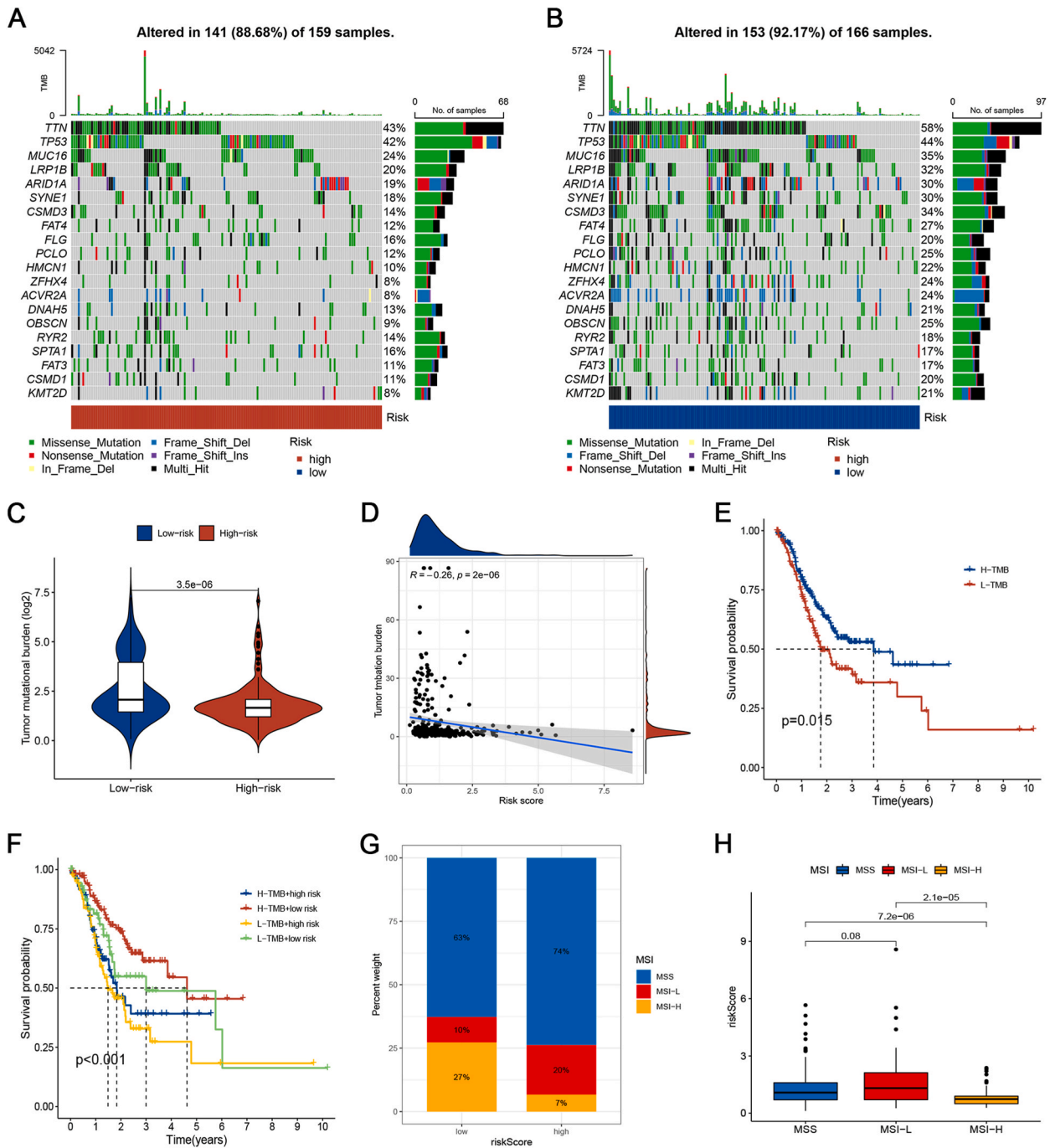**Fig. 11.** Correlation analysis of CRG_score with TMB and MSI. (A, B) The plot of genetic changes caused by somatic mutations was created using high and low CRG_scores. (C) The difference of TMB in different CRG_score groups. (D) Correlation of TMB with CRG_scores. (E) The OS between the low- and high-TMB groups was analyzed using Kaplan-Meier analysis. (F) Survival analysis was conducted on four patient groups, which were stratified based on both TMB and CRG_score. (G) The difference in the proportion of different microsatellite instability status in two risk subgroups. (H) The difference of CRG_score in different microsatellite instability status groups.

groups. Notably, the low-risk group (92.17%) exhibited a higher likelihood of gene mutations than the high-risk group (88.68%). Furthermore, we examined the correlation between the risk score and TMB. The results indicate that the low-risk groups exhibited greater TMB than the high-risk groups (Fig. 11C, $P < 0.001$), suggesting that immunotherapy may be more advantageous for patients with a low-risk profile. Spearman's correlation analysis revealed a negative correlation between the CRG_score and TMB ($R = -0.26$, $P < 0.001$; Fig. 11D). To investigate the influence of the TMB status on the prognosis of patients with GC, we performed survival

analysis among various TMB subcategories. Patients with high TMB exhibited a more favorable prognosis than patients with low TMB (Fig. 11E, $P = 0.015$). Subsequently, we merged TMB and CRG_score to conduct survival analysis on patients with GC. This analysis showed that the low-risk group + low TMB score group had the worst prognosis (Fig. 11F, $P < 0.001$). Moreover, the differences in the MSI status between the two groups were compared. Fig. 11G shows that the percentage of patients with MSI-High (MSI-H) was lower in the high-risk group (7 %) than in the low-risk group (27%). Additionally, the MSI-H group exhibited the lowest CRG_score in comparison to the remaining two groups (Fig. 11H).

3.11. Validation of the signature gene expressions in GC tissues

The expression levels of the nine signature genes in GC tissues were compared with those in the adjacent normal tissues using qRT-PCR. The results indicate that the expression of COL8A1, MKX, SGCE, ASCL2, CDC42EP5, COMP, and CXCL13 was upregulated in GC tissues compared to that in adjacent normal tissues. Meanwhile, the expression of FLNA and PTGIS was downregulated in GC tissues compared to that in adjacent normal tissues (Fig. 12).

4. Discussion

GC exhibits significant heterogeneity, resulting in diverse clinical outcomes and varying treatment responses of patients. To address this issue, we investigated the potential role of cuproptosis in impeding the progression of GC. Consequently, we developed an innovative cuproptosis-associated indicator to facilitate risk stratification and personalized treatment prognosis. Our analysis initially focused on examining variations in gene expression levels and genetic mutation profiles among the distinct CRGs. By applying unsupervised clustering techniques to CRG transcriptome expression levels, we identified two separate CRG subtypes, specifically CRG clusters A and B. Notably, patients belonging to cluster A exhibited a worse prognosis despite having higher levels of immune infiltration than those in cluster B. Additionally, we identified 678 DEGs between the two CRG subtypes and classified them into three gene clusters. Notably, The significant variations in OS among these three gene subtypes, indicated a strong correlation between genes and CRG clusters.

We then established a CRG_score associated with the patient's clinical outcomes and characteristics of TME cell infiltration in GC. Patients were categorized into two risk subgroups based on the CRG_score. Indeed, a low CRG_score of patients, characterized by a high mutation burden, MSI-H, and activation of immunity, indicated a favorable OS. Conversely, patients with high-risk exhibited a low mutation burden, MSI-H, and inhibition of immunity, indicating a worse OS. Additionally, patients with low CRG_scores had a high IPS and a low TIDE scores, indicating that they may respond better to immunotherapy. Finally, we developed a prognostic nomogram incorporating CRG_score, age, N stage, T stage, and CRG_score to further enhance the clinical application of the model. These findings are of clinical significance, emphasizing the potential of CRG expression profiles in accurately predicting patient outcomes and therapeutic responses.

The intricate interactions within the immune system play a crucial role in tumor development, making it a key focus of therapeutic interventions in GC. The TME is mainly composed of stromal and immune cells, and its scores are linked to the clinical characteristics and prognosis of GC [27–29]. Tumor heterogeneity mainly stems from variations in tumor composition and gene expression. Unraveling the diversity of immune responses to tumors is crucial for identifying potent combinational targets to enhance the efficacy of GC treatment. In our study, we observed a negative correlation between the high-risk group and CD8^{+} T cells, M1 macrophages, and activated memory CD4^{+} T cells; conversely, a positive correlation was observed between the high-risk group and resting memory CD4^{+} T cells, M2 macrophages, resting mast cells, and monocytes. Notably, T cells have been found to influence GC progression through antitumor responses [30]. CD8^{+} T cells can lyse and kill tumor cells by releasing cytotoxic factors [31]. Many studies have confirmed that high-density CD8^{+} T cells significantly correlate with improved prognosis in patients with GC [32,33]. Consistent with the
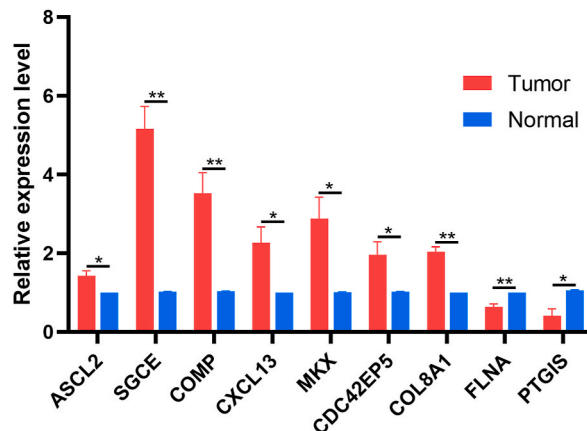

Fig. 12. The expression levels of the 9 signature genes in GC tissues and adjacent normal tissues.

findings of these previous studies, our results suggest that high-risk patients with poor prognosis had a lower CD8$^+$ T cell density.

Monocytes circulating in the bloodstream can migrate to various tissues, where they undergo differentiation into either macrophages or dendritic cells. Depending on their mode of activation and function, macrophages can be broadly classified into two primary types: M1 and M2 macrophages. Notably, some studies suggest that M2 macrophages have the potential to enhance tumor development in GC [34,35]. In line with these findings, we observed higher infiltrating levels of M2 macrophages in the high CRG_score subgroup, indicating a potentially low TME immunoreactivity. This observation may explain the worse OS outcomes of high-risk patients. We propose that the CRG_score could serve as a novel immune indicator in GC, aiding clinicians in identifying patients who might benefit from immunotherapy.

We investigated variations in the TME based on the CRG_score, which could potentially indicate the diverse immune advantages of ICI treatment. This investigation was conducted using the TIDE and IPS. The TIDE score is associated with two distinct ways through which the immune system evades anti-tumor responses: the malfunction of cytotoxic T lymphocytes (CTLs) that infiltrate tumors and the exclusion of CTLs. TIDE scores are indicative of the likelihood of anti-tumor immune evasion and serve as an indicator of the potential effectiveness of ICI treatment [23]. We found that patients with a low CRG_scores tended to have lower TIDE scores than those with higher CRG_scores. Consequently, it indicated a likelihood of experiencing a higher ICI response. The immune checkpoint system (IPS) is primarily linked to a few immune checkpoints, namely PD-1, PD-L1, and CTLA-4. Previous studies have shown that avelumab (an anti-PD-1 drug) exhibits anticancer effects and is well-tolerated in patients with GC during clinical trials of immunotherapy. It is often utilized as a maintenance therapy after achieving disease control with standard chemotherapy [36]. Consistent with these findings, the low-risk group identified by the CRG_score exhibited significantly higher IPS values. Taken together, the TIDE and IPS analyses based on the CRG_score indicate its potential to distinguish between different outcomes in patients undergoing immunotherapy. The CRG_score may serve as a valuable tool in the selection of ICI treatments in clinical trials, proving a theoretical basis for cancer treatments. The utilization of this prognostic model contributes to expediting the advancement of individualized cancer treatments.

Based on the clinical trials, studies have indicated that immune therapy yields positive outcomes in patients with GC, particularly when administered before the disease was managed with standard chemotherapy [37–39]. Our objective was to determine whether the combined use of chemotherapy and immunotherapy in GC improved effectiveness, thereby warranting further investigation. Hence, we investigated the responsiveness to different medications in individuals belonging to two distinct risk categories based on the CRG_score. The findings of our study indicate that the low-risk category exhibited a significantly high likelihood of responding positively to ICI treatment. Additionally, we identified a robust correlation between low-risk classification and the effectiveness of specific medications, such as Gefitinib and Metformin. Therefore, future research should focus on exploring integrated therapeutic approaches for patients with GC. Notably, the CRG_score predictive model identified medications that showed promise for treating GC under certain circumstances.

Despite the merits of our findings, few limitations exist in this study. The results were retrospectively formulated and confirmed using publicly accessible databases, necessitating further studies to assess the practicality of the observed pattern in patients diagnosed with GC. Additionally, we verified the expression volume at the tissue level, although the sample size was limited. Our objective was to gather additional samples to assess the observed distinctive pattern during immunotherapy. Additionally, we aimed to determine whether there were any differences in the advantages of immunotherapy between populations categorized as high- and low-risk.

5. Conclusions

We evaluated the potential roles of CRGs in the TME of GC tissues by analyzing selected cohorts from GEO and TCGA using an array of in silico methods. Two clusters with distinct clinical outcomes and immune characteristics were identified. Subsequently, a CRG-related signature and prognostic nomogram were developed. High tumor mutation burden, increased microsatellite instability-high, and immune activation, along with good survival probability and increased immunoreactivity to ICIs were distinguishing features of low CRG_scores. Our analysis revealed potentially relevant mechanisms through which CRGs might affect the tumor-immune-stromal microenvironment and clinical outcomes of patients with GC that predict their therapeutic response to immunotherapy and targeted therapy. These findings are of clinical importance and provide a rationale for exploiting the expression profiles of CRGs to accurately predict outcomes and responses to therapy in patients with GC.

Ethics approval and consent to participate

As this work benefited from the public database, informed consent was not applicable.

Data availability statement

The original contributions presented in the study are included in the article/Supplementary Material. Further inquiries can be directed to the corresponding authors.

Funding

CRediT authorship contribution statement

Yatao Wang: Writing – review & editing, Writing – original draft, Visualization, Supervision, Formal analysis, Data curation. **Fengqin Guo:** Writing – review & editing, Writing – original draft, Visualization, Supervision, Formal analysis, Data curation. **Wei Song:** Writing – review & editing, Writing – original draft, Visualization, Supervision, Formal analysis, Data curation. **Wenyi Guo:** Writing – original draft, Software, Resources, Investigation, Data curation. **Junwei Shao:** Writing – original draft, Software, Resources, Data curation. **Yanliang Liu:** Writing – review & editing, Writing – original draft, Validation, Supervision, Project administration, Funding acquisition, Conceptualization.

Declaration of competing interest

The authors declare that they have no known competing financial interests or personal relationships that could have appeared to influence the work reported in this paper.

Abbreviations

DEGs	differentially expressed genes
CRGs	cuproptosis-related genes
TME	tumor microenvironment
LASSO	least absolute shrinkage and selection operator (LASSO)
IPS	higher immunophenoscore
TMB	tumor mutational burden
MSI	microsatellite instability
TPM	transcripts per kilobase million
GSVA	Gene Set Variation Analysis
PCA	Principal component analysis
ROC	receiver operator characteristic
TAM	tumor-associated macrophages

Appendix A. Supplementary data

Supplementary data to this article can be found online at https://doi.org/10.1016/j.heliyon.2024.e24411.

References

[1] H. Sung, J. Ferlay, R.L. Siegel, M. Laversanne, I. Soerjomataram, A. Jemal, et al., Global cancer statistics 2020: GLOBOCAN estimates of incidence and mortality worldwide for 36 cancers in 185 countries, CA A Cancer J. Clin. 71 (3) (2021 May) 209–249.
[2] X. Rao, C. Zhang, H. Luo, J. Zhang, Z. Zhuang, Z. Liang, et al., Targeting gastric cancer stem cells to enhance treatment response, Cells 11 (18) (2022 Sep 10).
[3] E. Koren, Y. Fuchs, Modes of regulated cell death in cancer, Cancer Discov. 11 (2) (2021 Feb) 245–265.
[4] J. Li, F. Cao, H.L. Yin, Z.J. Huang, Z.T. Lin, N. Mao, et al., Ferroptosis: past, present and future, Cell Death Dis. 11 (2) (2020 Feb 3) 88.
[5] D. Bertheloot, E. Latz, B.S. Franklin, Necroptosis, pyroptosis and apoptosis: an intricate game of cell death, Cell. Mol. Immunol. 18 (5) (2021 May) 1106–1121.
[6] E.J. Ge, A.I. Bush, A. Casini, P.A. Cobine, J.R. Cross, G.M. DeNicola, et al., Connecting copper and cancer: from transition metal signalling to metalloplasia, Nat. Rev. Cancer 22 (2) (2022 Feb) 102–113.
[7] P. Tsvetkov, S. Coy, B. Petrova, M. Dreishpoon, A. Verma, M. Abdusamad, et al., Copper induces cell death by targeting lipoylated TCA cycle proteins, Science 375 (6586) (2022 Mar 18) 1254–1261.
[8] V. Oliveri, Selective targeting of cancer cells by copper ionophores: an overview, Front. Mol. Biosci. 9 (2022) 841814.
[9] Y. Feng, J.W. Zeng, Q. Ma, S. Zhang, J. Tang, J.F. Feng, Serum copper and zinc levels in breast cancer: a meta-analysis, J. Trace Elem. Med. Biol. 62 (2020 Dec) 126629.
[10] T. Atakul, S.O. Altinkaya, B.I. Abas, C. Yenisey, Serum copper and zinc levels in patients with endometrial cancer, Biol. Trace Elem. Res. 195 (1) (2020 May) 46–54.
[11] S. Mao, S. Huang, Zinc and copper levels in bladder cancer: a systematic review and meta-analysis, Biol. Trace Elem. Res. 153 (1–3) (2013 Jun) 5–10.
[12] E. Theodoratou, M. Timofeeva, X. Li, X. Meng, J.P.A. Ioannidis, Nature, nurture, and cancer risks: genetic and nutritional contributions to cancer, Annu. Rev. Nutr. 37 (2017 Aug 21) 293–320.
[13] E. Jafari Maskouni, T. Jamalvandi, F. Tabatabaei, S. Bourenjan Shirazi, H. Saadati, A. Letafati, et al., Association between Epstein-Bar virus and colorectal cancer: a systematic review and meta-analysis, Microb. Pathog. 179 (2023 Jun) 106087.
[14] A. Letafati, S.H. Mozhgani, A. Marjani, A. Amiri, Z. Siami, M. Mohammaditabar, et al., Decoding dysregulated angiogenesis in HTLV-1 asymptomatic carriers compared to healthy individuals, Med. Oncol. 40 (11) (2023 Oct 4) 317.
[15] S. Ghorbani, V. Tambrchi, R. Farzi, A. Khatami, R.N. Samiei, H. Saadati, et al., Association between human Epstein–Barr virus and brain cancer: a systematic review and meta-analysis, Future Virol. 18 (8) (2023) 537–545.
[16] M.D. Wilkerson, D.N. Hayes, ConsensusClusterPlus: a class discovery tool with confidence assessments and item tracking, Bioinformatics 26 (12) (2010 Jun 15) 1572–1573.
[17] K. Yoshihara, M. Shahmoradgoli, E. Martínez, R. Vegesna, H. Kim, W. Torres-Garcia, et al., Inferring tumour purity and stromal and immune cell admixture from expression data, Nat. Commun. 4 (2013) 2612.
[18] S. Hänzelmann, R. Castelo, J. Guinney, GSVA: gene set variation analysis for microarray and RNA-seq data, BMC Bioinf. 14 (2013 Jan 16) 7.
[19] M.E. Ritchie, B. Phipson, D. Wu, Y. Hu, C.W. Law, W. Shi, et al., Limma powers differential expression analyses for RNA-sequencing and microarray studies, Nucleic Acids Res. 43 (7) (2015 Apr 20) e47.

[20] T. Wu, E. Hu, S. Xu, M. Chen, P. Guo, Z. Dai, et al., clusterProfiler 4.0: a universal enrichment tool for interpreting omics data, Innovation 2 (3) (2021 Aug 28) 100141.

[21] N. Simon, J. Friedman, T. Hastie, R. Tibshirani, Regularization paths for cox's proportional hazards model via coordinate descent, J. Stat. Software 39 (5) (2011 Mar) 1–13.

[22] A.M. Newman, C.L. Liu, M.R. Green, A.J. Gentles, W. Feng, Y. Xu, et al., Robust enumeration of cell subsets from tissue expression profiles, Nat. Methods 12 (5) (2015 May) 453–457.

[23] P. Jiang, S. Gu, D. Pan, J. Fu, A. Sahu, X. Hu, et al., Signatures of T cell dysfunction and exclusion predict cancer immunotherapy response, Nat. Med. 24 (10) (2018 Oct) 1550–1558.

[24] P. Charoentong, F. Finotello, M. Angelova, C. Mayer, M. Efremova, D. Rieder, et al., Pan-cancer immunogenomic analyses reveal genotype-immunophenotype relationships and predictors of response to checkpoint blockade, Cell Rep. 18 (1) (2017 Jan 3) 248–262.

[25] A. Mayakonda, D.C. Lin, Y. Assenov, C. Plass, H.P. Koeffler, Maftools: efficient and comprehensive analysis of somatic variants in cancer, Genome Res. 28 (11) (2018 Nov) 1747–1756.

[26] D. Maeser, R.F. Gruener, R.S. Huang, oncoPredict: an R package for predicting in vivo or cancer patient drug response and biomarkers from cell line screening data, Briefings Bioinf. (6) (2021 Nov 5) 22.

[27] J.E. Bader, K. Voss, J.C. Rathmell, Targeting metabolism to improve the tumor microenvironment for cancer immunotherapy, Mol. Cell 78 (6) (2020 Jun 18) 1019–1033.

[28] Y. Xiao, D. Yu, Tumor microenvironment as a therapeutic target in cancer, Pharmacol. Ther. 221 (2021 May) 107753.

[29] D.C. Hinshaw, L.A. Shevde, The tumor microenvironment innately modulates cancer progression, Cancer Res. 79 (18) (2019 Sep 15) 4557–4566.

[30] M. Wei, D. Shen, S. Mulmi Shrestha, J. Liu, J. Zhang, Y. Yin, The progress of T cell immunity related to prognosis in gastric cancer, BioMed Res. Int. 2018 (2018) 3201940.

[31] J. Galon, D. Bruni, Approaches to treat immune hot, altered and cold tumours with combination immunotherapies, Nat. Rev. Drug Discov. 18 (3) (2019 Mar) 197–218.

[32] Y. Wang, C. Zhu, W. Song, J. Li, G. Zhao, H. Cao, PD-L1 expression and CD8(+) T cell infiltration predict a favorable prognosis in advanced gastric cancer, J. Immunol. Res. 2018 (2018) 4180517.

[33] T. Tuncel, B. Karagoz, A. Haholu, A. Ozgun, L. Emirzeoglu, O. Bilgi, et al., Immunoregulatory function of HLA-G in gastric cancer, Asian Pac. J. Cancer Prev. APJCP : APJCP. 14 (12) (2013) 7681–7684.

[34] V. Gambardella, J. Castillo, N. Tarazona, F. Gimeno-Valiente, C. Martínez-Ciarpaglini, M. Cabeza-Segura, et al., The role of tumor-associated macrophages in gastric cancer development and their potential as a therapeutic target, Cancer Treat Rev. 86 (2020 Jun) 102015.

[35] Y. Chen, S. Zhang, Q. Wang, X. Zhang, Tumor-recruited M2 macrophages promote gastric and breast cancer metastasis via M2 macrophage-secreted CHI3L1 protein, J. Hematol. Oncol. 10 (1) (2017 Feb 1) 36.

[36] H.C. Chung, H.T. Arkenau, J. Lee, S.Y. Rha, D.Y. Oh, L. Wyrwicz, et al., Avelumab (anti-PD-L1) as first-line switch-maintenance or second-line therapy in patients with advanced gastric or gastroesophageal junction cancer: phase 1b results from the JAVELIN Solid Tumor trial, J. Immunother. Cancer 7 (1) (2019 Feb 4) 30.

[37] K. Li, A. Zhang, X. Li, H. Zhang, L. Zhao, Advances in clinical immunotherapy for gastric cancer, Biochim. Biophys. Acta Rev. Canc 1876 (2) (2021 Dec) 188615.

[38] S.S. Joshi, B.D. Badgwell, Current treatment and recent progress in gastric cancer, CA A Cancer J. Clin. 71 (3) (2021 May) 264–279.

[39] S. Li, W. Yu, F. Xie, H. Luo, Z. Liu, W. Lv, et al., Neoadjuvant therapy with immune checkpoint blockade, antiangiogenesis, and chemotherapy for locally advanced gastric cancer, Nat. Commun. 14 (1) (2023 Jan 3) 8.